

Focus errors from tracking sodium layer altitude variations with laser guide star adaptive optics for the Thirty Meter Telescope

Glen Herriot^a, Paul Hickson^b, Brent Ellerbroek^c, Jean-Pierre Véran^a,
Chiao-Yao She^d, Richard Clare^d, Doug Looze^e

^aHerzberg Institute of Astrophysics – National Research Council (Canada)

^bUniversity of British Columbia (Canada), ^cThirty Meter Telescope Project,

^dColorado State University, ^eUniversity of Massachusetts

ABSTRACT

Laser guide star (LGS) adaptive optics systems for extremely large telescopes must handle an important effect that is negligible for current generation telescopes. Wavefront errors, due to improperly focusing laser wavefront sensors (WFS) on the mesospheric sodium layer, are proportional to the square of the telescope diameter. The sodium layer, whose mean altitude is approximately 90 km, can move vertically at rates of up to a few metres per second; a few seconds lag in refocusing can substantially degrade delivered image quality (15 m of defocus can cause 120 nm residual wavefront error on a 30-m telescope.) As well, the range of temporal frequencies of sodium altitude focus, overlaps the temporal frequencies of focus caused by atmospheric turbulence. Only natural star wavefront sensors can disentangle this degeneracy. However, applying corrections with representative focus mechanisms having modest control bandwidths, causes appreciable tracking errors. In principle, electronic offsets measured by natural guide star detectors could be rapidly applied to laser WFS measurements, but to provide useable sky coverage, integrating sufficient photons causes an unavoidable time delay, again resulting in potentially serious focus tracking errors. However, our analysis depends on extrapolating to temporal frequencies greater than 1 Hz from power spectra of sodium profile time series taken at 1-2 minute intervals. In principle, with a pulsed laser, (e.g. 3- μ s pulses) and dynamic refocusing on a polar-coordinate CCD, this focus tracking error may be eliminated. This result is an additional benefit of dynamic refocusing beyond the commonly recognized amelioration of LGS WFS spot elongation.

Keywords: Adaptive Optics, sodium layer, focus tracking, TMT, pulsed laser, dynamic refocusing

1. INTRODUCTION

At about 90 km altitude there is a layer of sodium, deposited by the in-fall of micro-meteorites, and removed from below by chemical reactions. The mean altitude of the sodium layer tends to show a slow variation punctuated by sporadic events possibly corresponding to the burn-up of a micrometeorite, which shifts the mean altitude rapidly¹⁴. These variations follow a power law as discussed in section 2. In section 3 we derive the focus error which results because an adap-

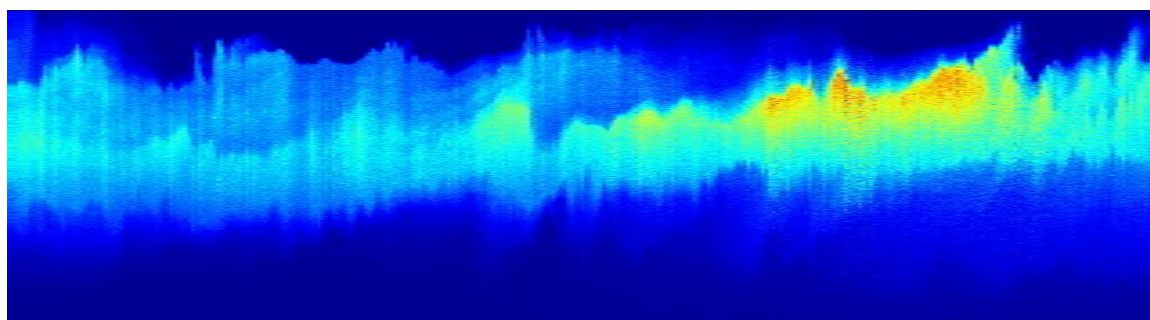


Figure 1 Profiles of Sodium return vs altitude and time. Each column of pixels shows a single 1-minute Lidar profile taken with the Purple Crow Lidar at the University of Western Ontario. The vertical axis ranges from 80 to 100 km and the total time along the horizontal axis is \sim 6 hours.

tive optics system's laser guide star wavefront sensors (LGS WFSs) will not be exactly focused at the current centroid

height of the sodium layer. The LGS WFSs can be refocused either electronically or mechanically by comparing the defocus measured on a natural guide star (NGS) with the defocus measured on the LGSs. However, on a Thirty Meter Telescope (TMT) one meter of error in the focus adjustment at the range of the sodium layer results in 8 nm RMS of focus wavefront error. This scale factor increases with the square of the diameter of the telescope, and therefore this effect has not received much attention in the past for LGS AO systems on 8- to 10-meter telescopes.

Note that the focus measurements, from NGS WFSs in instruments, drive electronic focus offsets to apply within the real time computer, to the LGS WFS measurements. On longer time scales these are off-loaded to refocus the zoom optics in a LGS WFS. For TMT we have estimated 18 nm RMS for the median “Sodium layer altitude tracking error.” For more information on the sodium layer servo tracking and a derivation of this error budget term, see section 4.

Since the absolute focus information is derived from an NGS measurement, this residual error analysis relies on using a sky coverage estimation tool. The limitation here comes from the low frame rate in the NGS WFS, ~90 Hz which, for 50% sky coverage, is the best tradeoff between read noise, photon noise and servo errors, both for tip/tilt and focus, explained in section 5.

Finally, we describe dynamic refocusing in section 6, and show how it eliminates the sodium focusing problem in section 7.

2. POWER SPECTRUM OF SODIUM ALTITUDE

The left panel of Figure 2 plots the mean height of profiles taken with a Lidar by Colorado State University on two different nights, and in two directions (zenith and 30 degrees off zenith.) While the profiles in two directions are correlated, there can be up to a kilometre difference in sodium altitude over the sky, and rapid vertical jumps of 5-10 m/s.

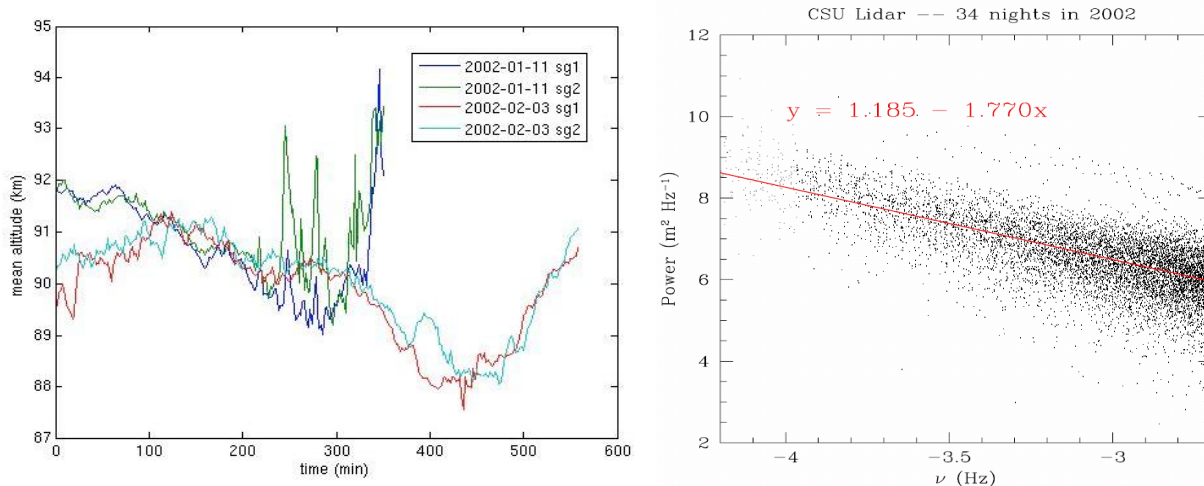


Figure 2 Left: Mean altitude of sodium layer on two nights, at zenith and 30 degrees away. Right: power spectra from 144 data sets (1-8 hr each) log-log scale, and best fit power law.

Notice that the largest jumps happen towards the end of the data series, consistent with the observation that meteors are more frequent near dawn as the earth faces oncoming particles. The right hand panel of Figure 2 shows the best fit through power spectra of sodium altitude measurements taken over 34 nights. The X and Y axes are log frequency and log power respectively. This best fit line was used to derive the residual defocus term in the error budget for the TMT facility AO system NFIRAOS⁴, assuming 90 Hz sampling to apply electronic focus offsets, discussed below. There are two important caveats:

1. Since the Lidar data were taken with 2-minute sampling, we are extrapolating 2-3 decades in frequency to determine most of this residual defocus in section 4.1. As a result, to verify these tentative conclusions, during the preliminary design phase for TMT, we expect to obtain higher frequency data. For example, the vertical resolution of the Purple Crow Lidar is 24 m, which could be coarsened to allow temporal resolution as fine as 8-second intervals.

- The defocus power at the higher temporal frequencies can vary by at least a decade in amplitude; sometimes the residual defocus appears to completely dominate the error budget.

Figure 3 compares the power spectra of wavefront variance caused by defocus from atmospheric turbulence, and defocus due to the best fit model, from Figure 2, of altitude variations of the sodium layer, scaled into the same units using equation (4) for a 30-m telescope. Notice that the two disturbances' temporal frequencies overlap.

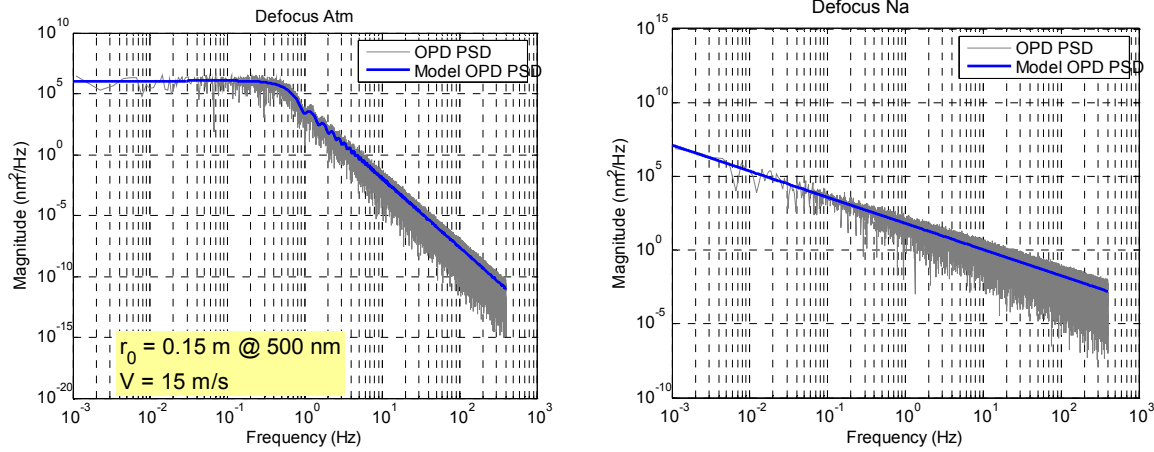


Figure 3 Comparison of power spectra of wavefront variance (nm^2/Hz) due to defocus from atmospheric turbulence (left) and the defocus due to altitude variation of sodium (right), scaled in the same units assuming a 30-m telescope. The focus disturbances from the two sources occur over an overlapping range of frequencies.

3. WAVE FRONT ERROR FROM UNCERTAINTY OF MEAN SODIUM ALTITUDE

Consider a point source located on the telescope axis a distance h (e.g. the sodium layer at 90 km) from the entrance pupil. In the pupil, the wavefront from this source is spherical with radius of curvature R . The longitudinal position of a point on the wavefront, at a transverse distance r from the axis is

$$z = \frac{r^2}{2h} - \frac{r^4}{8h^3} + \dots \quad (1)$$

When focused on the source, the telescope images this spherical wave to a point at the focus. Now suppose that the source is moved a small distance Δh in the longitudinal direction. The source then gives rise to a spherical wavefront with radius of curvature $h + \Delta h$. The difference between the original and the new wavefront is

$$\begin{aligned} \Delta z &= \frac{\partial z}{\partial h} \Delta h \\ &= -\frac{r^2}{2h^2} \Delta h \end{aligned} \quad (2)$$

If the telescope is not refocused, this term represents the wavefront error (optical path difference) as a function of transverse radial distance in the pupil. To find the wavefront variance, we average the squared error over the aperture

$$\begin{aligned} \sigma^2 &= \langle (\Delta z)^2 \rangle \\ &= \frac{4}{\pi D^2} \int_0^{D/2} (\Delta z)^2 2\pi r dr \end{aligned} \quad (3)$$

$$= \frac{2(\Delta h)^2}{D^2 h^4} \int_0^{D/2} r^5 dr$$

So the RMS wavefront error from defocus is

$$\sigma = \frac{1}{8\sqrt{3}} \frac{D^2}{h^2} \Delta h \quad (4)$$

Evaluating equation (4) for $D = 30$ m, and $h = 90$ km gives a wavefront error σ of 8 nm rms for each meter of defocus Δh . For example, if a laser-beacon wavefront sensor was focused at an altitude of 90 km and the sodium layer was actually 15 m higher, then the measurement error would be 120 nm rms, the entire top-level wavefront error specification set in the science requirements for the facility AO system on the Thirty Meter Telescope.

Since the error grows as the square of the telescope diameter, sodium altitude variation has not been a problem for 8-m to 10-m telescopes, which can reposition their WFS fore optics sufficiently accurately on short enough time scales.

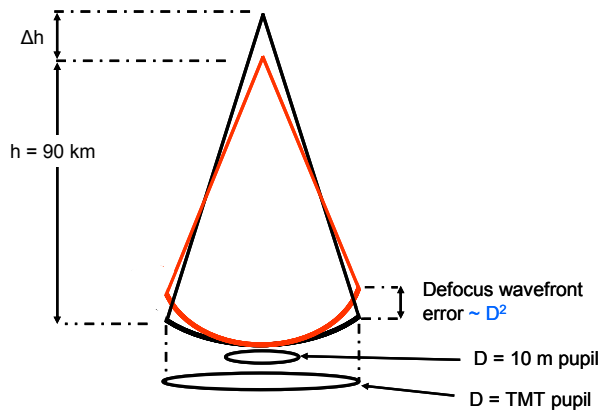


Figure 4 Illustration of increased sensitivity of extremely large telescopes to uncertainty in sodium layer altitude.

4. FOCUS TRACKING ARCHITECTURE

The absolute reference for focus in a laser guide star AO system must be a natural star, since the distance to the sodium layer is unknown. As described in section 5, to achieve good sky coverage (e.g. 50% probability of finding a natural guide star in the field of view to measure focus) means using relatively slow frame rates for NGS WFSs. Laser guide stars can detect atmospheric defocus on short time scales and be read more rapidly, but these measurements are confounded by the changing height of the sodium layer whose temporal frequencies overlap those of atmospheric turbulence. Ideally the LGS WFS should sense atmospheric turbulence and ignore sodium height changes.

To ignore sodium height, in practice means accurately focusing the WFSs onto the sodium layer. In a typical LGS AO system, the WFSs are continuously refocused optically by mounting them on translating stages or preceding the WFSs with a trombone or zoom optics whose task is to change focus while relaying a pupil image onto the lenslet arrays, of the wavefront sensor, with a constant magnification. For example, in the LGS zoom optics for NFIRAOS, the facility AO system for TMT, the most demanding lens is 50 kg and travels about 1 m to focus on the sodium layer ranging in altitude from 85 to 100 km while the telescope points from zenith to 65 degrees off-zenith. The bandwidth of this mechanism is about 0.1 Hz – too slow to track the sodium altitude precisely enough.

We have developed an electronic offsetting scheme, where we apply rapid NGS-based focus offsets to the measurements from the LGS WFS while the optical focus is slowly adjusted in a woofer-tweeter process⁵. Figure 5 is a Simulink model of our method. The simulation includes an atmospheric defocus disturbance, affecting both the natural and laser wavefront sensors, and a sodium altitude defocus that affects only the laser WFS.

The novel part is in the lower left of the figure, which blends the two (NGS & LGS WFSs) and in doing so, disregards the low temporal frequencies of focus from the LGS WFS and substitutes those with the slower, but more accurate NGS. The innovation is to subtract the LGS from the NGS measurements and then pass the difference through a low-pass Butterworth filter whose output is added back to the LGS focus signal as a focus offset. These offsets are available at the full frame rate of the LGS WFS. If we ignore the NGS for the moment, then from the point of view of the LGS WFS focus measurements, a low-pass filtered version of LGS focus is subtracted from the LGS focus signal. The net result is high pass filtered focus. I.e. the dc component (long term drift) is removed. Why go to this trouble instead of simply high pass filtering the LGS focus? The answer is that from the point of view of the NGS WFS focus signal, it sees a low-pass filter, before being added as an offset to the LGS focus; *but, the NGS filtering is exactly complementary to the LGS filtering*. Thus, the tradeoff between sensing the atmospheric turbulence and rejecting sodium altitude variations can be optimized by adjusting the corner frequency of this single Butterworth filter.

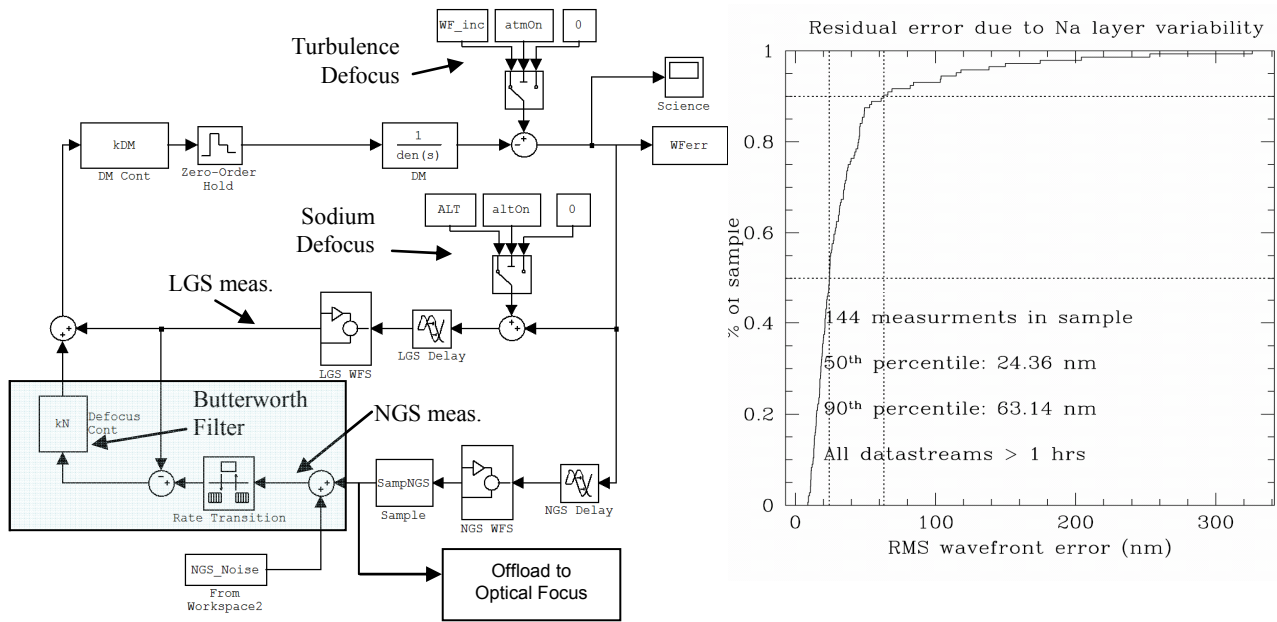


Figure 5 Left: Simulink diagram illustrating blending NGS focus measurements to add electronic offsets to LGS WFS. Right: Cumulative distribution of residual wavefront error due to defocus servo lag in 144 measurements; each measurement is a sodium altitude data set of 1-12 hours length.

Given the 800 Hz frame rate expected for the LGS WFSs on NFIRAOS and the 90 Hz median frame rate of the NGS WFS, described in the next section, we find that the optimal blending filter is typically 20-40 Hz. As the sample rate for the NGS WFS increases when brighter guide stars are fortuitously available, then the blending filter bandwidth increases. This allows rejecting more of the spurious defocus signal caused variations in sodium-layer altitude.

This approach is in contrast to conventional LGS AO systems on 8-m to 10-m telescopes that do not include the processing depicted in the lower left corner of Figure 5. The focus measurements from the NGS WFSs are used only to directly control the LGS focusing optics. By slowly refocusing the LGS optics to keep a NGS WFS focus at null, the dc and low frequency components of LGS focus are effectively ignored on long time scales. Therefore, the net result is a high-pass filter applied to the LGS focus measurements, but its cut-on frequency is very low – set by the mechanical bandwidth of focusing optics. For a thirty-meter telescope, the WFS focus optics are more massive, and yet as we have seen, it is more important to make rapid adjustments.

4.1 Cumulative distribution of residual defocus wavefront error

The signal processing architecture can be viewed as a rejection transfer function, capable of ignoring low temporal frequencies but incapable of reducing high frequency LGS focus errors. Using this rejection transfer function between sodium layer defocus and delivered wavefront error, we processed 144 data sets from the Colorado State University Lidar, shown previously as power spectra in Figure 2. The result is a cumulative probability distribution of residual defocus

wavefront error from imperfectly tracking the sodium layer (right panel of Figure 5.) Each data point is calculated from a time record, from one to 12 hours duration, of sodium return intensity vs. altitude. The median residual error was 24.4 nm rms, slightly higher than the 18 nm from the best fit through all the power spectra. Ninety per cent of the measurements have less than 63 nm rms focus error, but in 5% of the cases, the wavefront errors from AO systems on thirty-meter telescopes would be completely dominated by sodium layer focus tracking errors. The chief cause is the integration time delay to get enough photons for acceptable signal to noise on the NGS WFS – although electronic offsets can take effect instantly, it takes time to determine them.

5. SKY COVERAGE IMPLICATIONS

The baseline for client instruments, fed by the TMT AO system NFIRAOS, is to have a suite of two tip/tilt sensors and one 2x2 Shack-Hartmann WFS, to measure anisoplanatism, image distortion and rotation, as well as tip/tilt and focus.

In reference 10, the tradeoff of sky coverage versus tip, tilt and focus errors is presented. A Monte Carlo sky coverage model provides fast simulations of the wavefront error using guide star constellations generated from star-count models. While the primary purpose is to evaluate tip/tilt performance for TMT AO systems, nonetheless, since focus is measured from the same natural stars, the best compromise sample rate is a function of residual tip/tilt and focus errors together with noise and disturbance inputs.

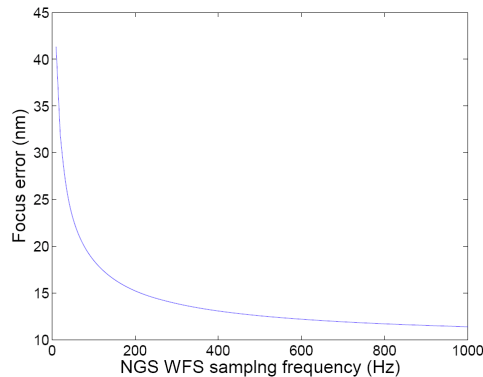


Figure 6 The sodium altitude focus wavefront error is reduced with brighter natural guide stars, allowing higher frame rates.

This model evaluates the overall tip/tilt error associated with each randomly generated NGS asterism, accounting for the combined effects of anisoplanatism, servo lag, WFS noise, telescope windshake, and any partial “sharpening” of the NGS images provided by the LGS AO system. For each simulated constellation, the model determines the optimal frame rate to balance the errors. Low-order (but tip-tilt removed) LGS WFS measurements are also included in the formulation of the tip/tilt estimation algorithm, since these measurements provide additional information on the 3-dimensional turbulence profile which is useful to reduce the estimation error due to anisoplanatism. The simulation includes T/T woofer-tweeter control and analysis of the residual errors resulting from using noisy, finite bandwidth NGS WFS focus measurements to keep the LGS WFSs focused on the varying range of the sodium layer. Figure 6 shows the residual defocus for different frame rates of electronic offsets derived from NGS WFS measurements, based on the best fit power spectrum of sodium altitude from Figure 2. Clearly faster is better, but the median optimized sample rate at the galactic pole is 90 Hz.

6. DYNAMIC REFOCUSING

As described above, laser guide star AO systems on extremely large telescopes are very sensitive to the changing altitude of the sodium layer. High speed readout of NGS focus sensors can provide electronic focus offsets to LGS wavefront sensors to reduce the problem. However, some of the time, especially near dawn, the variations in altitude are too rapid and natural stars are too faint (or NGS WFS detectors are too noisy) to determine offsets quickly enough.

Fortunately there is another solution, called dynamic refocusing, so far proposed as a cure for the laser spot elongation problem, but which also has the benefit of completely fixing the sodium altitude focus tracking problem.

To understand how this works, first we describe laser spot elongation, and how dynamic refocusing works to reduce this elongation, and finally how dynamic refocusing mitigates the sodium tracking issue. Figure 7 illustrates the well-known

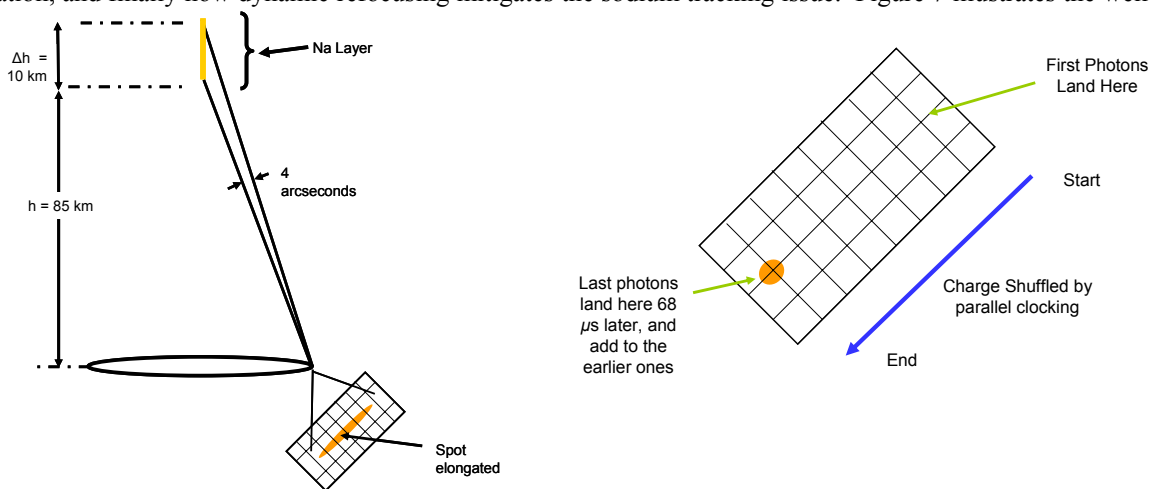


Figure 7 Left: LGS WFS spot elongation due to finite range distance and thickness of sodium layer. Right: dynamic refocusing by parallel clocking a polar coordinate CCD as photons arrive from a pulsed laser.

phenomenon where the outer edge of a large telescope's pupil sees a long laser streak in the 10-km thickness of the sodium layer. Consequently, the outer lenslets of a Shack-Hartmann wavefront sensor each create an elongated image of this streak on the CCD detector. These streaks are oriented radially, pointing away from the center of the array, (assuming that the laser launch telescope is behind the telescope secondary mirror) and increase in length to a maximum of 4 arcseconds, for subapertures at the outer edge of a 30-m telescope pupil.

Given the non-zero read-noise from the CCD pixels, together with background from Rayleigh scattering and sky brightness, spreading out the signal from the laser beacon across multiple pixels reduces the signal to noise ratio when measuring the spot positions in the radial direction, and requires more laser power. A polar coordinate CCD¹³ is under development to improve the situation. It has individual rectangular regions, one for each lenslet of the LGS WFS; each is oriented radially to minimize the number of pixels readout. CCD controllers typically read out rectangular regions of interest by parallel shifting followed by serial shifting; aligning the regions of interest with the streaks, reduces the total pixels to digitize, allowing more time to measure each pixel intensity and thus less read noise for a given frame time.

The long-term average nominal spot positions on the detector are determined by the focus setting of the WFS optics with respect to the mean height of the sodium layer. Then, if atmospheric turbulence causes defocus, then the LGS WFS spots move radially outward from the nominal position. This is indistinguishable from a change in height of the sodium layer, which also moves the spots radially.

The preceding describes the situation with a continuous wave laser. The authors of Ref. 13 propose a further refinement when using this CCD with a pulsed laser, illustrated in the right panel of Figure 7. If the laser was pulsed briefly, say for $3 \mu\text{s}$, the shot of photons would be 1 km long. The first photons arrive from the bottom of the sodium layer about $68 \mu\text{s}$ before the last ones arrive from the top of the layer (if pointing at zenith.) As well, due to the geometry, these first photons produce the outer end of the streaks on the LGS WFS CCD, and the last photons arrive at the inward end of the streak. If the parallel clock on the CCD were synchronized to shift the charge inwards during this $68\text{-}\mu\text{s}$ interval so that each arriving photon landed on the charge already produced, then the final image would be a nearly seeing-limited spot without elongation. The signal to noise would be equal for radial and azimuthal directions and the required laser power would be much smaller. This process is called Dynamic Refocusing.

Synchronizing the parallel clocking with the photon arrival, or Range Gating, is slaved to the current position of the LGS focus optics, which is continuously adjusted to null the NGS focus signal. At greater range distances due to increasing zenith angles or higher sodium altitude, the parallel clocking starts later after the laser pulse is launched and runs more slowly as the photons arrive.

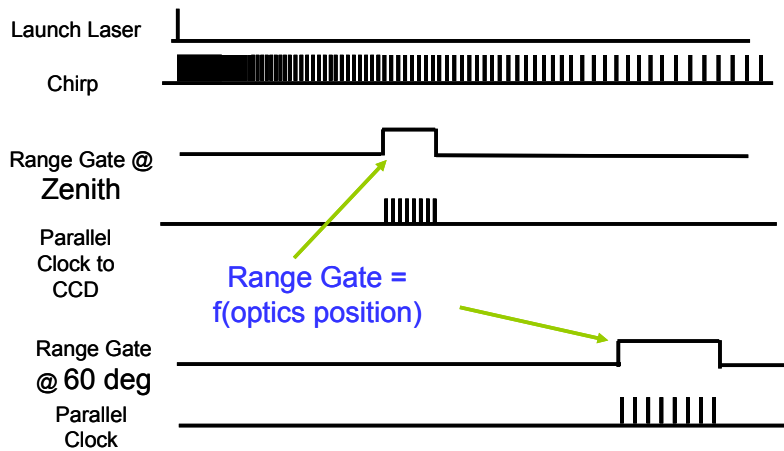


Figure 8 Range-gated chirped clocking waveforms

Figure 8 shows how this clocking might be accomplished. Each time a laser pulse is launched, a chirped clock begins running. It starts at a high frequency and slows down as time goes on. This clock waveform is the same for all zenith angles and range distances, and applies to all subapertures in an annular zone of constant distance from the laser launch telescope. Other zones closer to the launch telescope would have a slower chirped clock, and those further outward would have a faster clock, which slows proportionately more rapidly as well. Meanwhile, by monitoring the instantaneous position of the LGS WGS focusing optics, the time interval during which photons will arrive is known. Via a lookup table or a simple function of geometry the start and stop time of the range gate is determined. During the range gate, a section of the chirped clock waveform is sent to drive the parallel clocking of the CCD. This method has the advantage that it is purely digital and does not use drift-prone devices like voltage controlled oscillators (VCO). The timing is completely determined by geometry.

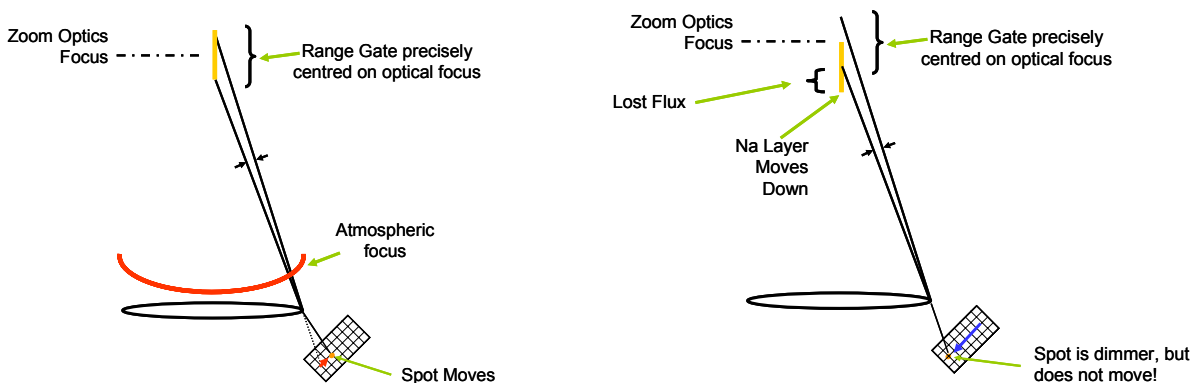


Figure 9 Dynamic Refocusing with a pulsed laser removes spot elongation. Focus changes from Atmospheric turbulence cause spot displacement – the signal of interest. Right: With Dynamic Refocusing, if the LGS WFS is mis-focused on the sodium layer, since the Range Gate matches the optical focus position, the Shack-Hartmann spots do not move. The LGS WFS is insensitive to time-varying sodium altitude

7. SODIUM TRACKING VIA DYNAMIC REFOCUSING

An interesting additional benefit of Dynamic Focusing with a pulsed laser is that it also solves the sodium focus tracking problem. Recall that the CCD Range Gate clocking is slaved to the current optical focus of the LGS WFS. Therefore, photo-electrons arising from the plane where the WFS is focused always end up in the same pixel (charge well) on the CCD (in the absence of turbulence.) Electrons generated from sodium emission on either side of best focus also finish in the same pixel. Only atmospheric turbulence causes them to reach neighboring pixels.

If the mean range of the sodium layer moves away from the current focus of the LGS WFS, the spots do not move, but some photons may be lost from one end of the range gate, seen in the right half of Figure 9. A slightly wider range gate, which may require a few more pixels in the radial dimension of each rectangular CCD region, would give margin to capture all the flux until the optical focus mechanism catches up. Note that these extra pixels are not digitized, and merely serve as a broader detector, so have no effect on signal to noise ratio.

The net result is a system that is insensitive to the confounding focus signal from sodium altitude variations described in the first part of this paper, and requires less total laser flux. However, of course, the required peak power of the laser is greatly increased, presenting a great technical challenge to laser designers. Nonetheless, the benefits in better signal to noise and measurement accuracy from centroiding smaller spots and from avoiding focus errors make this an enticing prospect.

8. CONCLUSIONS

A newly appreciated phenomenon becomes significant for adaptive optics on extremely large telescopes. Wavefront errors from mis-focusing LGS WFSs on the sodium layer grow with the square of the telescope diameter. Natural stars can provide a focus reference but correction is limited by mechanical response of correcting mechanisms, and most fundamentally by sample rates possible with available natural guide stars. The residual focus may add tens or sometimes even hundreds of nanometers wavefront error delivered to astronomical instruments.

However, our analysis depends on extrapolating to temporal frequencies greater than 1 Hz from power spectra of time series taken at 1-2 minute intervals. As a result, to verify these early conclusions, during the preliminary design phase for TMT, we hope to obtain higher frequency measurements of sodium profiles.

In principle, with a pulsed laser, (e.g. 3- μ s pulses) and dynamic refocusing on a polar-coordinate CCD, this focus tracking error may be eliminated. This result is an additional benefit of dynamic refocusing beyond the frequently discussed prevention of LGS WFS spot elongation.

ACKNOWLEDGEMENTS

The authors gratefully acknowledge the support of the TMT partner institutions. They are the Association of Canadian Universities for Research in Astronomy (ACURA), the Association of Universities for Research in Astronomy (AURA), the California Institute of Technology and the University of California. This work was supported, as well, by the Canada Foundation for Innovation, the Gordon and Betty Moore Foundation, the National Optical Astronomy Observatory, which is operated by AURA under cooperative agreement with the National Science Foundation, the Ontario Ministry of Research and Innovation, and the National Research Council of Canada.

REFERENCES

1. G. H. Sanders, J. E. Nelson, TMT status report, *this conference* [6267-60].
2. B.L. Ellerbroek, A Conceptual Design for the Thirty Meter Telescope Adaptive Optics Systems, *this conference* [6272-13].
3. D. Crampton, L. Simard, Instrument concepts and scientific opportunities for TMT, *this conference* [6269-67].
4. G. Herriot, P. Hickson, B. L. Ellerbroek, D.A. Andersen, R. A. Buchroeder, T. Davidge, D. A. Erickson, I. P. Powell, R. Clare, L. Gilles, C. Boyer, M. Smith, L. Saddlemyer, J-P Véran, "NFIRAOS: TMT narrow-field near-infrared facility adaptive optics," *this conference* [6272-24].
5. J.-P. Véran, G. Herriot, Woofer-tweeter tip-tilt control for NFIRAOS on TMT, *this conference* [6272-48].
6. G. Herriot, P. Hickson, J.-P. Véran, Focus errors from tracking sodium layer altitude variations with laser guide star adaptive optics for the Thirty Meter Telescope, *this conference* [6272-52].
7. L. Gilles, Laser Guide Star Shack-Hartman Wavefront Sensor Modeling: Matched Filtering, Wavefront Sensor Non-Linearity, and Impact of Sodium Layer Variability for the Thirty Meter Telescope, *this conference* [6272-57].

8. L. Gilles, Laser Guide Star Multi-Conjugate Adaptive Optics Performance of the Thirty Meter Telescope with Elongated Beacons and Matched Filtering, *this conference*[6272-169].
9. L. Gilles, Multi-Conjugate Adaptive Optics Performance Comparison of Wavefront Reconstruction and Fitting Algorithms for the Thirty Meter Telescope: MGPCG, FDPCG, and Order N Tomography, *this conference* [6272-110].
10. R. M. Clare, Sky coverage and tip/tilt error analysis for the thirty meter telescope, *this conference* [6272-107].
11. C. Boyer, TMT Adaptive Optics Systems Control Architecture, *this conference* [6272-35].
12. R. R. Joyce, The laser guide star facility for the Thirty Meter Telescope, *this conference* [6272-51].
13. Beletic, James W., Sean Adkins, Barry Burke, Robert Reich, Bernie Kosicki, Vyshnavi Suntharalingham, Charlie Bleau, Ray DuVarney, Richard Stover, Jerry Nelson, Francois Rigaut, "The Ultimate CCD for Laser Guide Star Wavefront Sensing on Extremely Large Telescopes", *Scientific Detectors for Astronomy 2005, Springer Dordrecht 2006*.
14. C. O'Sullivan, R. M. Redfern, N. Ageorges, H.-C. Holstenberg, W. Hackenberg, T. Ott, S. Rabien, R. Davies, A. Eckart, "Short timescale variability of the mesospheric sodium layer, *Exp. Astron. 10: 147-156, 2000*